

# BLAEs – I. Resolving the UV-continuum in Lyman alpha emitting galaxies between redshift 2 to 3 with gravitational lensing

E. Ritondale,<sup>1</sup> A. N. Other,<sup>2</sup> Third Author<sup>2,3</sup> and Fourth Author<sup>3</sup>

<sup>1</sup>Max Planck Institute for Astrophysics, Karl-Schwarzschild-Strasse 1, D-85740 Garching, Germany

Accepted XXX. Received YYY; in original form ZZZ

## ABSTRACT

Lyman-alpha emitters (LAEs) are low-mass, high specific star formation rate galaxies that are thought to be predominantly responsible for the reionisation of the Universe. In spite of their importance, it is extremely difficult to characterise in detail all but the brightest, most massive of these galaxies; this is unsatisfactory, since the faint LAE population is expected to contribute significantly to the reionisation. Here we present a study of a new sample of 20 strongly lensed Ly- $\alpha$  emitting galaxies at  $z \sim 2.3$ , where we take advantage of the lensing magnification (typically a factor of about 20) to characterise some of the physical properties of low star-formation rate LAEs for the first time.

**Key words:** gravitational lensing – galaxies: structure

## 1 INTRODUCTION

Lyman-alpha emitting galaxies (LAEs) represent a population of star-forming systems with very large Ly $\alpha$  equivalent widths and some of the highest specific star-formation rates (sSFR) in the Universe, and these low-mass galaxies are thought to be predominantly responsible for the reionisation of the Universe. However, it is extremely difficult to characterise these galaxies in detail because they are intrinsically very faint. Typical LAE galaxies have strong star-formation, high-ionisations, and are typically low metallicity; these properties, combined with a (mostly) low dust content, allow for the escape of a large fraction of Ly $\alpha$  photons. At redshift  $2 < z < 3$ , well-studied LAEs are typically at the bright end of this parameter space, being L<sub>\*</sub> galaxies with  $M_{*} \sim 10^9 M_{\odot}$  and typical SFRs of about 30 to  $100 M_{\odot}/\text{yr}$  (e.g. Erb et al. 2016), and investigations of lower-SFR objects have generally been limited to quantifying the properties of strong optical lines (e.g. Trainor et al. 2015). For example, Hagen et al. (2016) have recently shown that low-SFR LAEs ( $M_{*}$  as low as  $10^7 M_{\odot}$  and  $\text{SFR} \sim 1$  to  $100 M_{\odot}/\text{yr}$ , consistent with local-Universe *green pea* LAEs, e.g., Henry et al. 2015) have optical strong line (H $\alpha$  and [O iii]) properties consistent with optically-selected star-forming galaxies of the same masses at  $z \sim 2$ , but they are unable to directly determine the properties of these galaxies that may affect the UV escape fraction, including the gas metallicity, density, and kinematics, without additional very large investments in telescope time. Strong gravitational lensing can be used to overcome this limitation, but the difficulty is that most strongly lensed galaxies at  $z \sim 2$  are not LAEs, and at present the properties of only three lensed LAEs have been investigated in

detail (Christensen et al. 2012; Vanzella et al. 2016). Fortunately, new HST V -band observations of LAE galaxies selected from the BOSS survey have revealed a sample of strongly lensed systems at  $\langle z \rangle \sim 2.5$  for which the magnification effect could reveal the detailed structure of these LAEs at scales around 100 pc. Our subsequent lens modelling shows that the typical lensing magnification of these objects is  $\mu \sim 20$  and, after accounting for this magnification, these objects are compact galaxies with SFRs of  $\sim 12 M_{\odot}/\text{yr}$  (i.e., a factor of 3 to 8 lower than previous detailed studies).

In this paper, we use strong gravitational lensing to go beyond the current limits in angular resolution to investigate the size and structure and Lyman alpha emitting galaxies at high redshift on 100–500 pc-scales. Our study is based on the sample of candidate gravitational lenses that were selected from the BOSS Emission Line Lens Survey (BELLS) by Shu et al. (2016a). To summarise,  $1.4 \times 10^6$  galaxy spectra from the Baryon Oscillation Spectroscopic Survey (BOSS) of the Sloan Digital Sky Survey-III were inspected to search for Lyman alpha emission lines at a higher redshift than the dominant early-type galaxy in the spectrum. From this search, Shu et al. (2016a) selected twenty-one highest quality targets with source redshifts between  $z \sim 2$  to 3 for follow-up imaging with the *HST*. This selection method is based on the successful technique used by the Sloan Lens ACS Survey (SLACS) to find over eighty-five gravitational lensed star-forming galaxies at lower redshifts (Auger et al. 2009; Bolton et al. 2008), and has recently been applied by Shu et al. (2016b) to find a Lyman alpha emitting galaxy at redshift 2.701 that is gravitationally lensed by two elliptical galaxies at redshift 0.331.

Our paper is arranged as follows. In Section 2, we present the high angular resolution *HST* observations of the rest-frame ultraviolet continuum emission from the BELLS sample of candidate

\* E-mail: elisa@mpa-grarching.mpg.de

Lyman alpha emitting galaxies, from which we select the seventeen sources of our BOSS Lyman alpha emitters (BLAEs) sample. Using these data, the gravitational lens mass models and reconstructed source surface brightness distributions of the sample are determined in Section 3. From these source reconstructions, we investigate the intrinsic properties of the rest-frame ultra-violet continuum emission from the sample in Section 4. Here, we also study the properties of the stacked optical spectrum of the sample. We compare with other samples of Lyman alpha emitters in the literature and discuss our results in Section 5. Finally, in Section 6 we present our conclusions.

## 2 OBSERVATIONS

The BELLS sample was observed with the *HST* using the WFC3 camera and the F606W filter ( $\lambda_c = 5887 \text{ \AA}$ ;  $\Delta\lambda = 2182 \text{ \AA}$ ) between 2015 November and 2016 May (GO: 14189; PI: Bolton). In total, twenty one candidate gravitationally lensed Lyman-alpha emitting galaxies from the Shu et al. (2016a) sample were observed for about 2600 s each. As their redshifts span from  $z \sim 2.1$  to 2.8 and given the transmission curve of the F606W filter, these observations probed the rest-frame ultraviolet emission from young massive stars between 1250 and 2230  $\text{\AA}$ .

The data were retrieved from the *HST* archive and processed using the ASTRODRIZZLE task that is part of the DRIZZLEPAC package. Cut-out images for each target are shown in Fig. 1. Out of the twenty one candidates, three turned out not to be strong gravitational lenses with clear multiple images of the same background galaxy (SDSS J0054+2944, SDSS J1116+0915 and SDSS J1516+4954). Also, SDSS J2245+0040 is not included in our final sample because the uncertain nature of the deflector, which appears to be a spiral galaxy, made identifying the emission from the lensed Lyman alpha emitting galaxy challenging without additional colour information. Therefore, the final BLAEs sample used for our analysis contains seventeen gravitationally lensed Lyman-alpha emitting galaxies. The details of the sources in our final sample and the *HST* data that we will use are given in Table 1.

## 3 LENS MODELLING

### 3.1 Lens modelling procedure

The gravitational lens modelling and source reconstruction of each system was performed using the Bayesian pixelated technique developed by Vegetti & Koopmans (2009). Briefly, the mass density distribution of the lens is parametrized with an elliptical power-law profile (plus external shear) with a total of eight free parameters,

$$\kappa(x, y) = \frac{\kappa_0 \left(2 - \frac{\gamma}{2}\right) q^{\gamma-3/2}}{2 \left(q^2 (x^2 + r_c^2) + y^2\right)^{(y-1)/2}}, \quad (1)$$

where  $\kappa$  is the dimensionless surface mass density (as a function of position  $x, y$ ),  $\kappa_0$  is the surface mass density normalization,  $q$  is the axial ratio of the elliptical mass distribution,  $\gamma$  is the radial slope of the mass density profile and  $r_c$  is the core-radius. In addition, the position angle of the elliptical mass distribution ( $\theta$ ), and the shear strength ( $\Gamma$ ) and positional angle ( $\Gamma_\theta$ ) is also solved for. The dimensionless surface mass density and the Einstein radius ( $R_{\text{ein}}$ )

are related to each other via,

$$R_{\text{ein}} = \left( \frac{\kappa_0 \left(2 - \frac{\gamma}{2}\right) q^{(\gamma-2)/2}}{3 - \gamma} \right)^{1/(\gamma-1)}. \quad (2)$$

The surface brightness distribution of the foreground gravitational lens is simultaneously modelled with the mass distribution and is parametrised using elliptical Sersic profiles given by,

$$I(r) = I_0 \exp \left[ \left( -bn \left( \frac{r}{R_e} \right)^{1/n} \right) - 1.0 \right], \quad (3)$$

where  $I(r)$  is the surface brightness at radius  $r$ ,  $I_0$  is the surface brightness normalization,  $R_e$  is the effective radius,  $n$  is the Sersic index and  $b$  is the axial ratio.

The surface brightness distribution of the (lensing corrected) background source is instead reconstructed using a magnification-adaptive Delaunay tessellation and is characterised by a form and level of regularisation,  $\mathbf{R}_s$  and  $\lambda_s$  (see Vegetti & Koopmans 2009; Vegetti et al. 2014, for a more detailed description). This provides a pixellated surface brightness distribution for the reconstructed source that is free from any parameterised assumptions, such as Sersic or Gaussian light profiles, that may not fully account for the clumpy nature of the rest-frame ultraviolet emission from the BLAEs sources.

The modelling procedure is performed in three steps: first we masked out the emission from the lens galaxy and, given the lensed surface brightness distribution  $\mathbf{d}$ , we optimize for the lens mass parameters  $\boldsymbol{\eta} = \{\kappa_0, \theta, q, x, y, \gamma, \Gamma, \Gamma_\theta\}$  and the source regularisation level by maximising the posterior probability density,

$$P(\lambda_s, \boldsymbol{\eta} | \mathbf{d}, \mathbf{R}_s) = \frac{P(\mathbf{d} | \lambda_s, \boldsymbol{\eta}, \mathbf{R}_s) P(\lambda_s, \boldsymbol{\eta})}{P(\mathbf{d} | \mathbf{R}_s)}. \quad (4)$$

At each step of this optimization, the corresponding most probable source  $s$  is obtained by maximising the probability density distribution,

$$P(s | \mathbf{d}, \lambda_s, \boldsymbol{\eta}, \mathbf{R}_s) = \frac{P(\mathbf{d} | s, \boldsymbol{\eta}) P(s | \lambda_s, \mathbf{R}_s)}{P(\mathbf{d} | \lambda_s, \boldsymbol{\eta}, \mathbf{R}_s)}. \quad (5)$$

Then, using this as a starting point, we parametrise the surface brightness distribution of the lens galaxy as a sum of multiple elliptical Sersic profiles, and optimise for the corresponding parameters,  $\boldsymbol{\eta}_l = \{I_0, R_e, n, b, \theta\}$  together with the background source surface brightness distribution. In the third and final step, we optimise simultaneously for the mass and the light distribution of the deflector and the source regularisation level.

The resulting models for the lens- and source-plane light distributions are presented in Fig. 2, the gravitational lens mass model parameters are given in Table 1 and the Sersic surface brightness distributions of the lens galaxies are given in Table 2.

### 3.2 Notes on the individual lens models

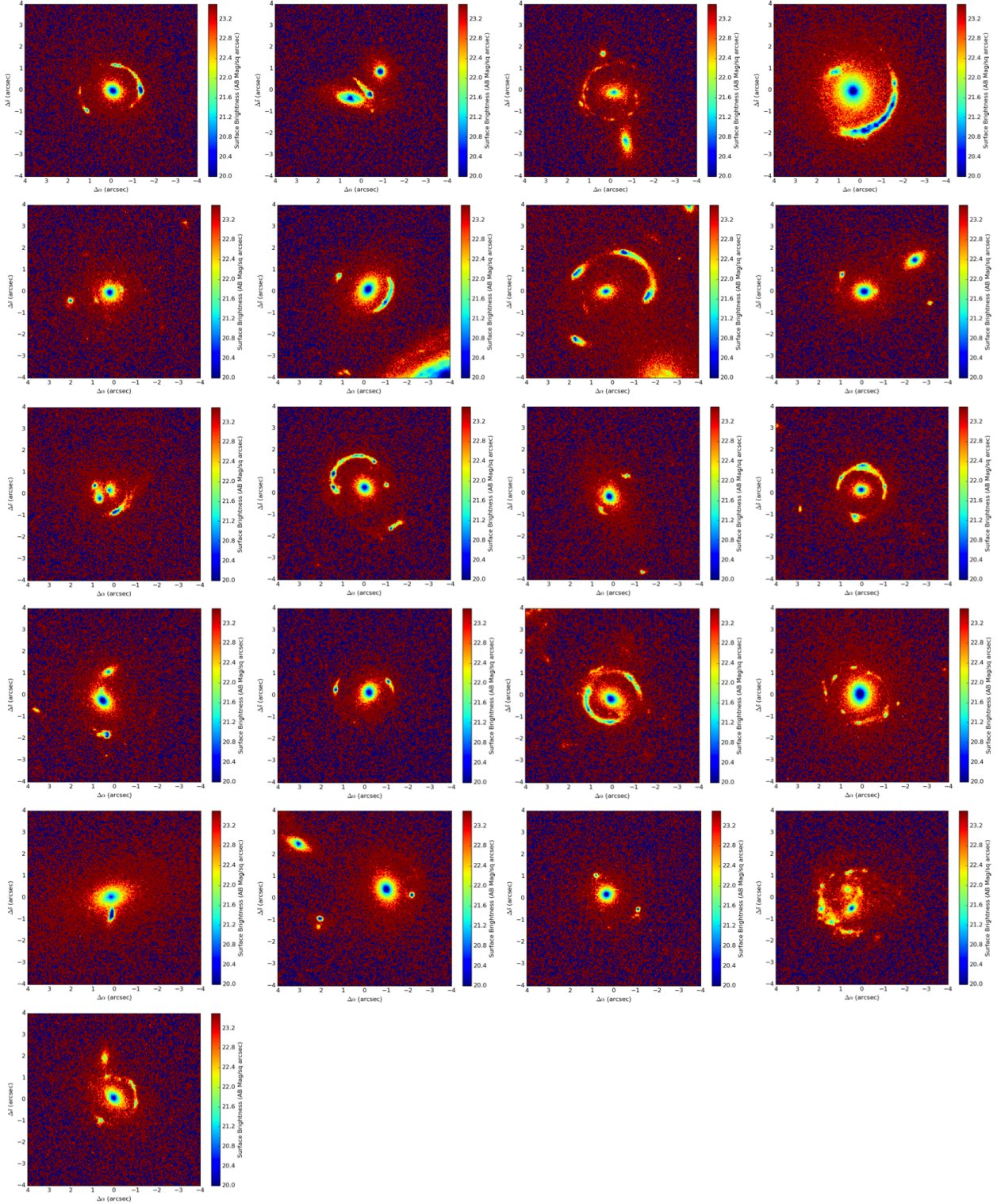
## 4 INTRINSIC PROPERTIES OF THE RECONSTRUCTED LAE GALAXIES

## 5 DISCUSSION

## 6 CONCLUSIONS

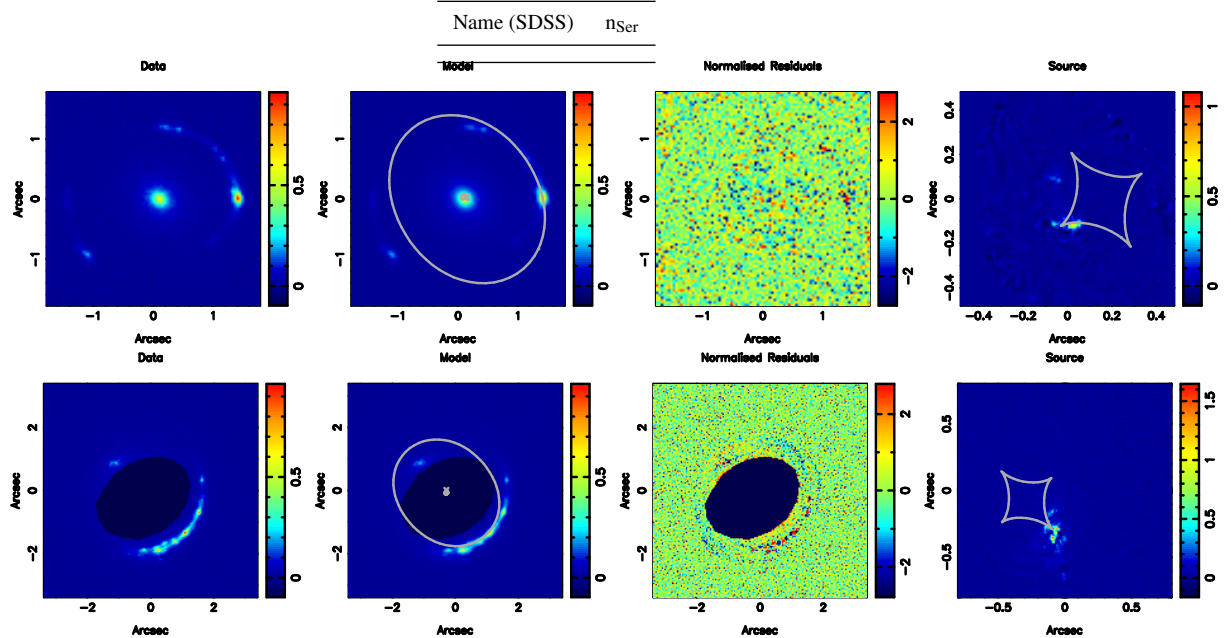
## REFERENCES

- Auger M. W., Treu T., Bolton A. S., Gavazzi R., Koopmans L. V. E., Marshall P. J., Bundy K., Moustakas L. A., 2009, *ApJ*, **705**, 1099



**Table 1.** Details of the BLAEs sample used for our analysis and the derived gravitational lens mass models.

| Name (SDSS)  | $z_{\text{lens}}$ | $z_{\text{src}}$ | $\lambda_{\text{rest}} [\text{\AA}]$ | Exp. Time [s] | $R_{\text{ein}} [\text{arcsec}]$ |
|--------------|-------------------|------------------|--------------------------------------|---------------|----------------------------------|
| J0029 + 2544 | 0.587             | 2.450            | 1706                                 | 2504          | 1.330                            |
| J0113 + 0250 | 0.623             | 2.609            | 1631                                 | 2484          | 1.225                            |
|              |                   |                  |                                      |               | 0.070                            |
|              |                   |                  |                                      |               | 0.173                            |
| J0201 + 3228 | 0.396             | 2.821            | 1540                                 | 2520          |                                  |
| J0237 – 0641 | 0.486             | 2.249            | 1812                                 | 2488          | 0.536                            |
| J0742 + 3341 | 0.494             | 2.363            | 1751                                 | 2520          | 1.208                            |
| J0755 + 3445 | 0.722             | 2.634            | 1620                                 | 2520          |                                  |
| J0856 + 2010 | 0.507             | 2.233            | 1821                                 | 2496          | 0.745                            |
| J0918 + 4518 | 0.524             | 2.344            | 1761                                 | 2624          |                                  |
| J0918 + 5104 | 0.581             | 2.403            | 1730                                 | 2676          |                                  |
| J1110 + 2808 | 0.607             | 2.399            | 1732                                 | 2504          | 0.985                            |
| J1110 + 3649 | 0.733             | 2.502            | 1682                                 | 2540          | 1.145                            |
| J1141 + 2216 | 0.586             | 2.762            | 1565                                 | 2496          | 1.281                            |
| J1201 + 4743 | 0.563             | 2.126            | 1883                                 | 2624          | 1.186                            |
| J1226 + 5457 | 0.498             | 2.732            | 1578                                 | 2676          |                                  |
| J1529 + 4015 | 0.531             | 2.792            | 1553                                 | 2580          |                                  |
| J2228 + 1205 | 0.530             | 2.832            | 1536                                 | 2492          | 1.270                            |
| J2342 – 0120 | 0.527             | 2.265            | 1803                                 | 2484          | 1.088                            |

**Table 2.** Add caption here. This table should contain the best parameters for the sersic models**Figure 2.** Models for the BLAEs gravitational lens systems. Each row shows (left) the input *HST* F606W imaging, (middle-left) the reconstructed model for lens-plane surface brightness distribution of the gravitational lensing galaxy and the gravitationally lensed BLAEs galaxy, (middle-right) the normalised image residuals between  $\pm 2.5\sigma$ , and (right) the reconstructed surface brightness distribution of the BLAEs galaxy. Shown in grey are the gravitational lens mass model critical curves in the lens-plane and the caustics in the source-plane.

Bolton A. S., Burles S., Koopmans L. V. E., Treu T., Gavazzi R., Moustakas

MNRAS, 442, 2017

L. A., Wayth R., Schlegel D. J., 2008, *ApJ*, 682, 964Shu Y., et al., 2016a, preprint, ([arXiv:1604.01842](https://arxiv.org/abs/1604.01842))

Shu Y., Bolton A. S., Moustakas L. A., Stern D., Dey A., Brownstein J. R.,

Burles S., Spinrad H., 2016b, *ApJ*, 820, 43Vegetti S., Koopmans L. V. E., 2009, *MNRAS*, 392, 945

Vegetti S., Koopmans L. V. E., Auger M. W., Treu T., Bolton A. S., 2014,

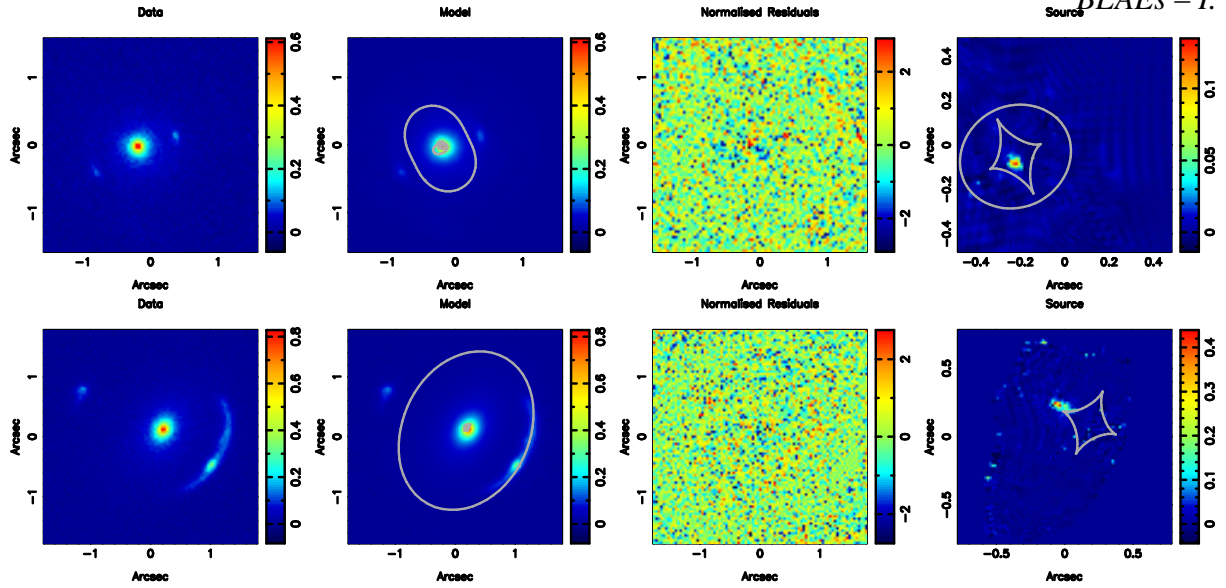


Figure 2 – continued

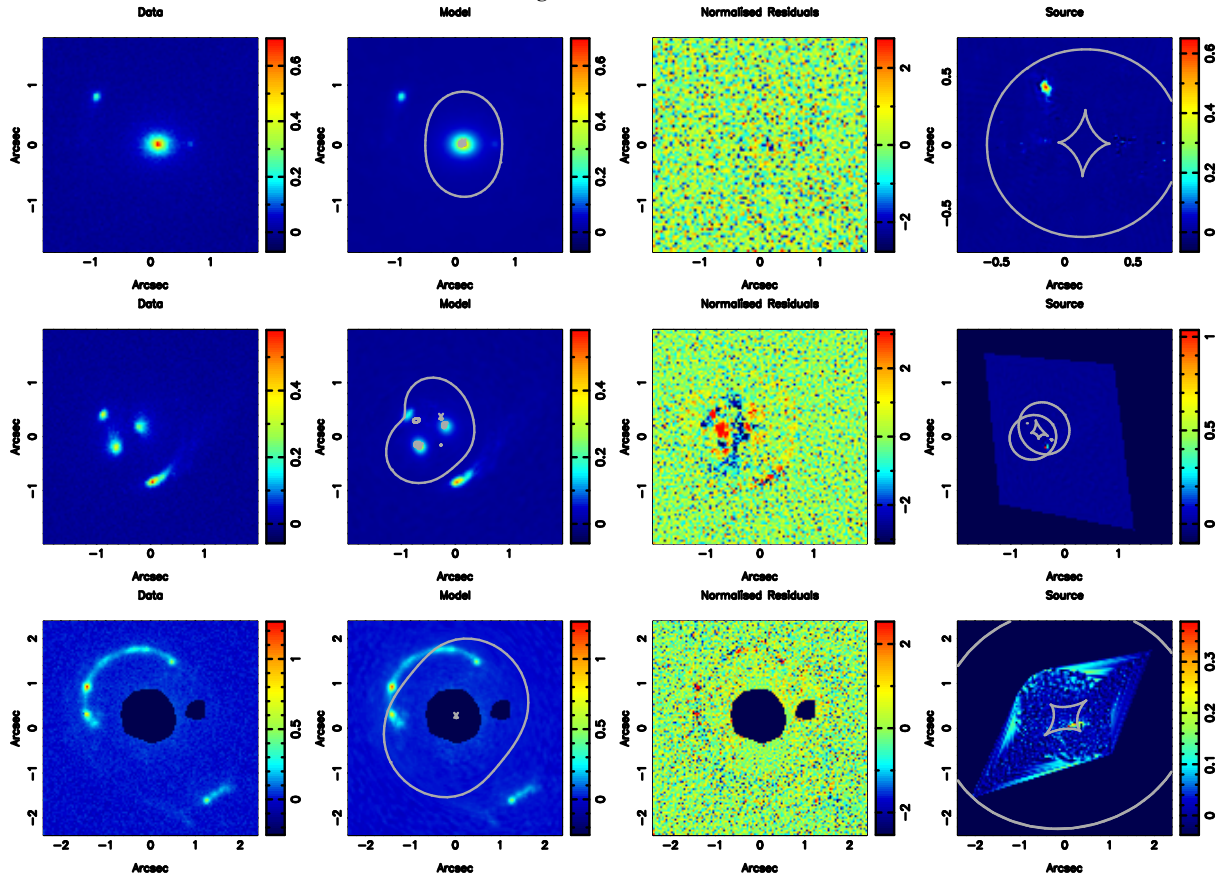
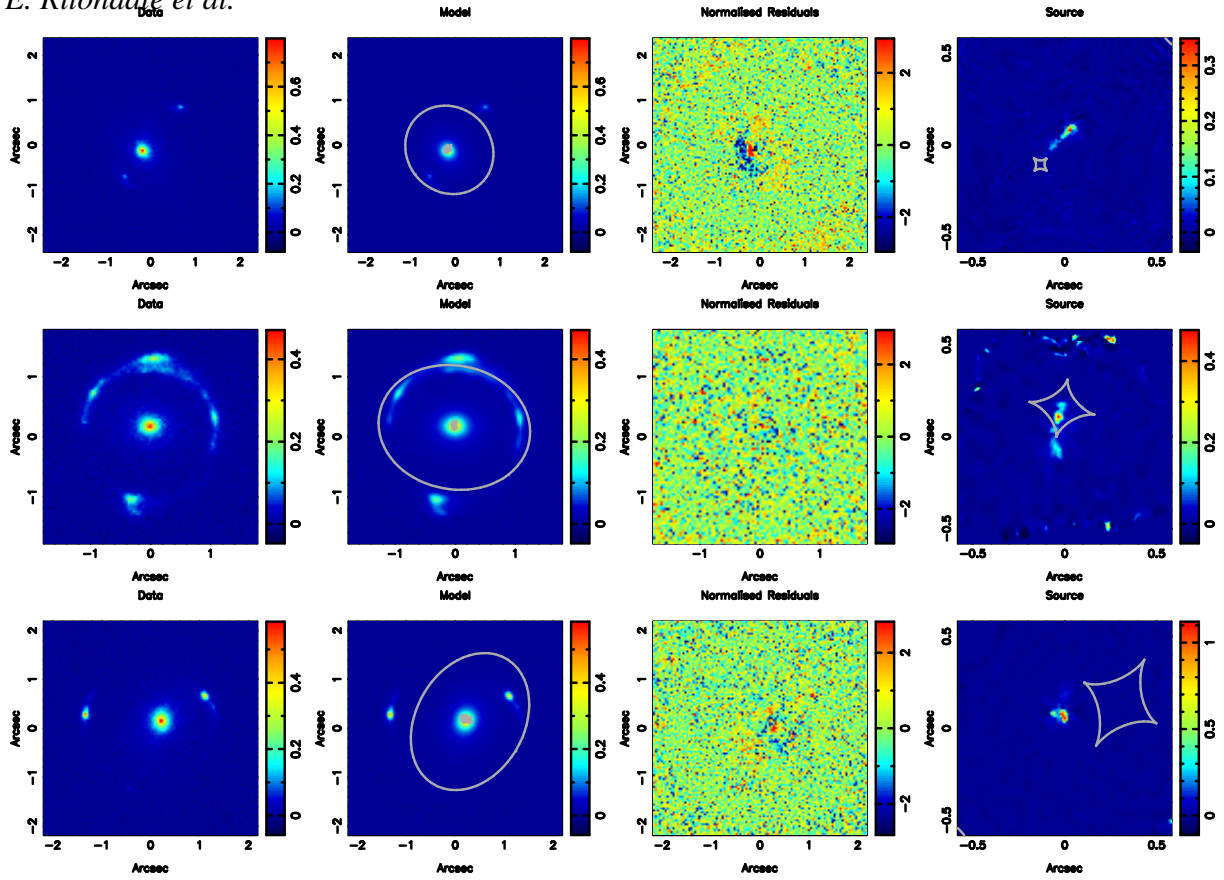


Figure 2 – continued

**Figure 2 – continued**

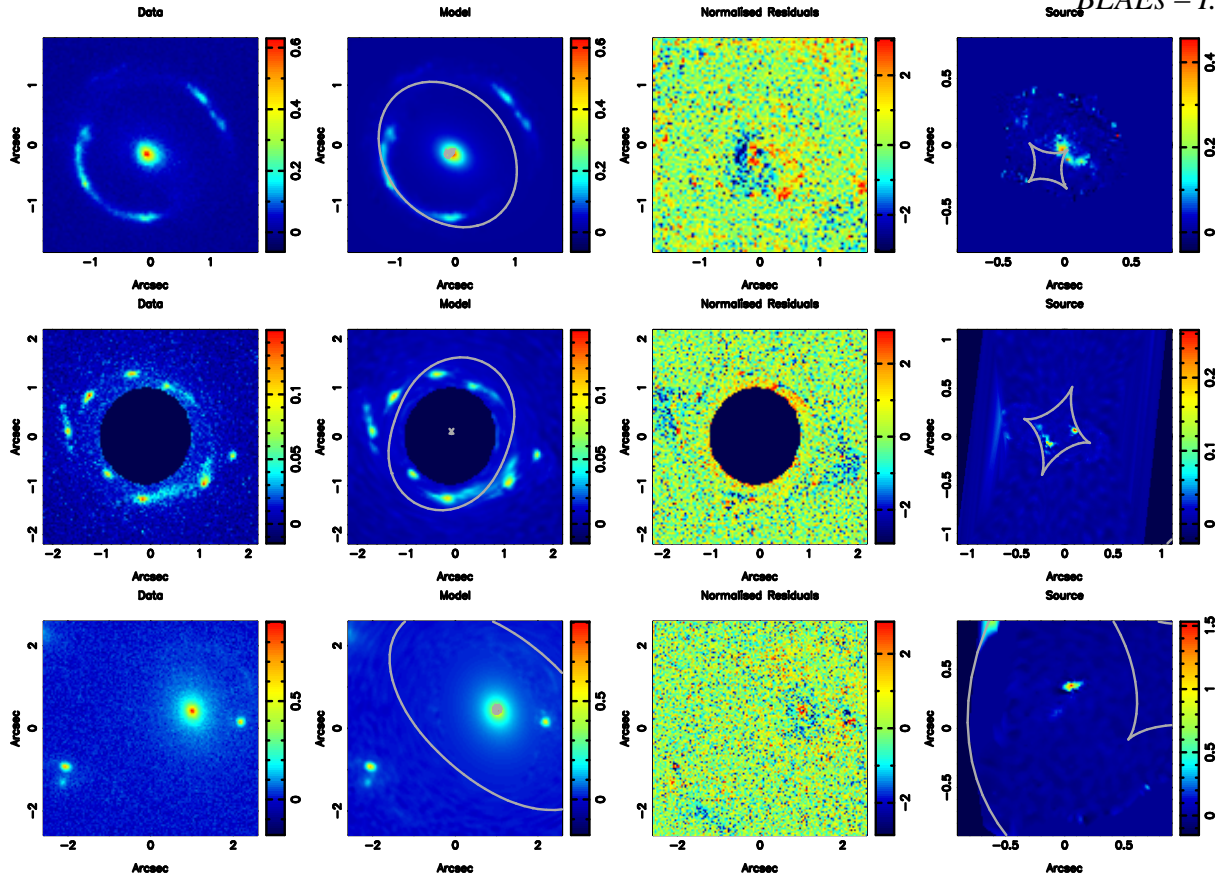


Figure 2 – continued

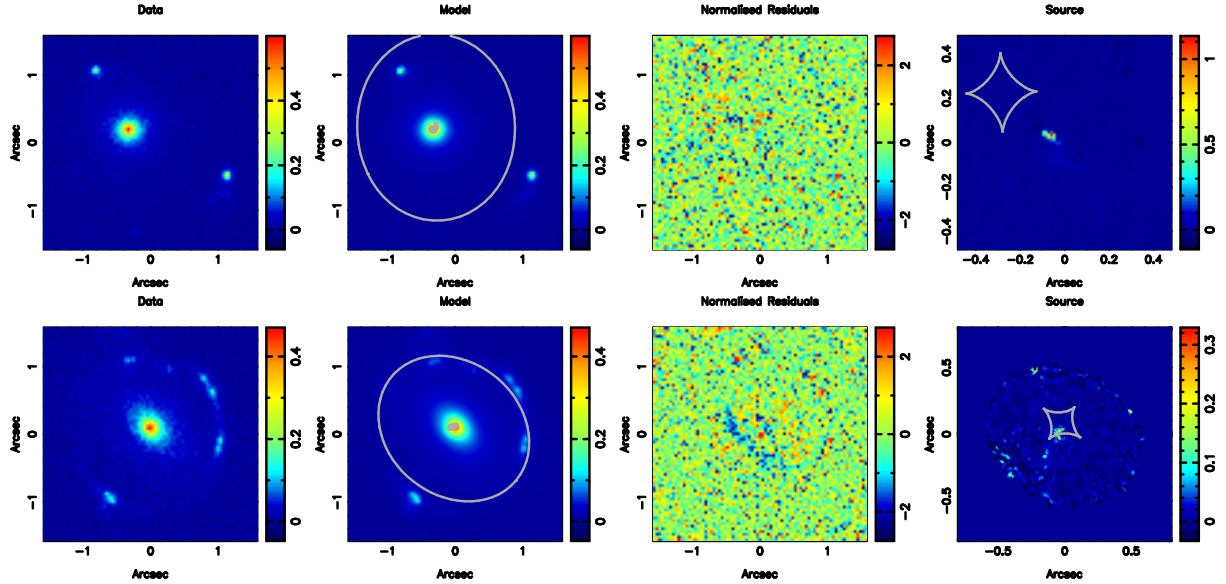


Figure 2 – continued